

BOSTON UNIVERSITY
GRADUATE SCHOOL OF ARTS AND SCIENCES

Dissertation

**ULTRA-HIGH PRECISION PHOTOMETRY OF OPEN CLUSTERS:
A STUDY OF STELLAR ACTIVITY IN OLD STARS**

by

MELISSA N. HAYES-GEHRKE

S.B., Massachusetts Institute of Technology, 1996

S.B., Massachusetts Institute of Technology, 1996

M.A., Boston University, 2001

Submitted in partial fulfillment of the
requirements for the degree of
Doctor of Philosophy

2004

© Copyright by
MELISSA N. HAYES-GEHRKE
2004

Approved by

First Reader

Kenneth A. Janes, Ph.D.
Professor of Astronomy

Second Reader

W. Jeffrey Hughes, Ph.D.
Professor of Astronomy

Third Reader

James Jackson, Ph.D.
Professor of Astronomy

ACKNOWLEDGMENTS

Many people have provided support and assistance for this research project.

My advisor, Ken Janes, has guided me in both research and teaching and made this project possible.

My thanks go to the many astronomers who took observations on behalf of this project: Ken Janes, Ken Yoss, Grant Miller, John Noble, Amanda Bosh, Brian Skiff, Svetlana Jorstad, Dan Eldredge, and Casey Law.

Finally, I am grateful my husband Bill had the patience for me to finish my degree. It's been a long road...

**ULTRA-HIGH PRECISION PHOTOMETRY OF OPEN CLUSTERS:
A STUDY OF STELLAR ACTIVITY IN OLD STARS**

(Order No.)

MELISSA N. HAYES-GEHRKE

Boston University, Graduate School of Arts and Sciences, 2004

Major Advisor: Kenneth A. Janes, Professor of Astronomy

ABSTRACT

The Sun varies in irradiance, or total flux, by about 0.1%, or 1 millimagnitude (mmag), over a period of days to weeks caused by the passage of active regions (composed of sunspots and associated phenomena) across its disk and over a period of years resulting from the solar cycle. Is the Sun a typical star at this level of activity? The ages of most nearby stars are poorly known, so they may not be suitable for comparison with the Sun. However, solar-type stars in star clusters have well-determined ages.

I present results of the search for stellar activity in four old star clusters with ages between 1.6 and 7 billion years. The data span a period of 8 yrs, consisting of more than 5 million individual magnitude measurements.

I selected a subset of active stars from the main sequence population by testing for the statistical significance of the photometric variability in each star. In the three youngest clusters, NGC 7789, NGC 6819, and M67, between 4% and 28% of the stars are significantly active on a rotational timescale with amplitudes of 6 to 10 mmag; no activity is seen on this timescale for the oldest cluster, NGC 188. On a yearly timescale, all of the clusters have a small fraction of active stars (3% to 19%) with amplitudes of 5 to 12 mmag. The lightcurves of individual stars show trends over the 8 year period reminiscent of the solar cycle. The data also show strong evidence that many more stars are active with amplitudes below the formal limits of detection.

Stellar activity in solar-type stars on the rotational timescale declines to amplitudes less than 1.5 mmag, the detection limit, by the age of the oldest cluster (7 billion years).

The activity in typical stars in the younger clusters has a much higher amplitude than is observed in the Sun, but is in good agreement with previous studies based on observations of younger stars.

Contents

Contents	vii
List of Tables	xii
List of Figures	xv
List of Acronyms	xxi
1 Introduction	1
1.1 The Sun and Its Activity	2
1.2 Why is the Sun Active?	3
1.3 The Activity of Other Stars	4
1.3.1 Extending the Magnetic Dynamo Model	4
1.3.2 Sun-Like Stars	6
1.3.3 IC 2391	8
1.3.4 IC 2602	8
1.3.5 α Persei	9
1.3.6 IC 4665	9
1.3.7 The Pleiades	9
1.3.8 The Coma Star Cluster	10
1.3.9 The Hyades	10
1.3.10 M67	11
1.3.11 Current Activity vs. Age Relationship	11
1.4 Distinguishing Stellar Activity	13
1.5 Technical Challenge	18

1.5.1	General CCD Data Reduction Procedure	18
1.5.2	Strategies for Maximizing S/N	20
1.5.3	Specialized Procedures	23
1.5.4	Examples of High-Precision Photometry	24
1.6	Goals	27
2	A Program for Evaluating Stellar Activity vs. Age	29
2.1	Program Objects	29
2.1.1	NGC 7789	30
2.1.2	NGC 6819	31
2.1.3	M67	32
2.1.4	NGC 188	32
2.2	Differential Ensemble Photometry	33
2.3	Data Requirements	34
2.3.1	Noise Budget	35
2.3.2	Time Baseline and Precision	38
3	Observational Program: Phase I	40
3.1	Observing Program	40
3.1.1	Mt. Laguna Observatory Observations	43
3.1.2	Perkins Telescope Observations	43
3.1.3	BU Queue	45
3.2	Reduction Process	46
3.2.1	Basic Data Reduction Using IRAF	46
3.2.2	SPS Photometry	51
3.2.3	Astrometric Transformation with <i>Astrometry</i>	58
3.2.4	Photometric Transformation with <i>Magmap</i>	59
3.2.5	Ensemble Photometry with <i>Diffmag</i>	59
3.3	Phase I Results: NGC 7789 as a Test Case	62

3.3.1	Photometric Errors or Stellar Activity?	62
3.3.2	An Activity Index: The Nightly Mean Differential Magnitudes	75
3.3.3	Power Spectra	82
3.3.4	Solar Analogs	86
3.3.5	Activity Index for Annual Mean Differential Magnitudes	90
3.3.6	Summary	93
3.4	Phase I Results for NGC 6819, M67 and NGC 188	96
3.4.1	NGC 6819	96
3.4.2	M67	96
3.4.3	NGC 188	98
3.5	Results of Phase I	134
3.6	Instrumental Limitations	135
4	Phase II	137
4.1	Observations	138
4.1.1	NGC 7789	138
4.1.2	NGC 6819	139
4.1.3	M67	139
4.1.4	NGC 188	139
4.1.5	Photometric Errors	139
4.2	Activity on the Nightly Timescale	142
4.2.1	The Activity Determination	142
4.2.2	Solar Analogs	152
4.3	Activity on the Yearly Timescale	155
4.3.1	The Activity Determination	155
4.3.2	Interesting Stars	160
4.3.3	Solar Analogs	162

5	Periodic Variables and Binary Sequences	185
5.1	Periodic Variable Stars	185
5.1.1	NGC 7789	186
5.1.2	NGC 6819	190
5.1.3	M67	194
5.1.4	NGC 188	196
5.2	Binary Sequences	200
6	Activity, Age and Color	206
6.1	Activity vs. Age	206
6.1.1	General Activity Level	209
6.1.2	Ensemble Error	211
6.1.3	α_v , A_v , and σ_{A_v} Distributions	212
6.2	Activity vs. Color	227
6.2.1	Correlation Between Activity Indices in Different Colors	227
6.2.2	Distribution of α_v , A_v , and σ_{A_v} by Spectral Type	230
6.3	Comparison to Other Solar-Type Stars	238
6.4	Rotation Periods	243
6.5	Long Term Trends	243
7	Summary	245
7.1	Individual Clusters	248
7.1.1	NGC 7789	248
7.1.2	NGC 6819	248
7.1.3	M67	249
7.1.4	NGC 188	249
7.2	Future Work	249
	Journal Abbreviations	253
	Bibliography	254

List of Tables

1.1	Photometric Variability on the Rotational Timescale	12
1.2	Photometric Variability on the Yearly Timescale	13
1.3	Ideal Amplitude of Variability by Filter	15
1.4	Scintillation Noise	22
2.1	Program Objects Summary	34
2.2	Calculated vs. SPS Magnitude Errors	37
2.3	Calculated vs. SPS Magnitude Errors	37
2.4	Minimum Nights Required	39
3.1	Phase I Observations	41
3.2	Phase I Observations – Continued	42
3.3	SPS Parameters	54
3.4	Phase I Observations of NGC 7789	63
3.5	NGC 7789 Observations on UT 1999 Sep 13	71
3.6	Statistical Properties of Data Sets from UT 1999 Sep 13.	72
3.7	Classification Scheme for Variability	78
3.8	Solar Analogs in NGC 7789.	87
3.9	Annual Mean Variables in NGC 7789	95
3.10	Phase I Observations of NGC 6819	97
3.11	Phase I Observations of M67	99
3.12	Phase I Observations of NGC 188	100
3.13	Summary of Activity for Phase I	111

3.14	Summary of Power Spectra for Phase I	111
3.15	Summary of Solar Analogs for Phase I	111
3.16	Solar Analogs in NGC 6819	114
3.17	Solar Analogs in M67	119
3.18	Solar Analogs in NGC 188	122
3.19	Summary of Annual Activity for Phase I	126
3.20	Annual Mean Variables in NGC 6819.	127
3.21	Annual Mean Variables in M67	131
3.22	Annual Mean Variables in NGC 188	133
3.23	Summary of the Activity of Main Sequence Stars in Clusters for Phase I.	135
4.1	Phase II Observations	138
4.2	Summary of Activity for Phase II	145
4.3	V vs B and V vs R Slopes for All Clusters	150
4.4	Results for Gaussian Fits of Nightly Magnitude Histograms for All Clusters, Phase II	154
4.5	Solar Analogs in NGC 7789, Phase II	154
4.6	Solar Analogs in NGC 6819, Phase II	157
4.7	Solar Analogs in M67, Phase II	161
4.8	Solar Analogs in NGC 188, Phase II	161
4.9	Phase I R Observations	161
4.10	Summary of Annual Activity for Phase II	165
4.11	V vs B, V vs R, and V vs I Slopes for All Clusters	165
4.12	Interesting Stars in NGC 7789 on the Yearly Timescale, Phase II	168
4.13	Interesting Stars in NGC 6819 on the Yearly Timescale, Phase II	168
4.14	Interesting Stars in M67 on the Yearly Timescale, Phase II	171
4.15	Interesting Stars in NGC 188 on the Yearly Timescale, Phase II	171
4.16	Solar Analogs in NGC 7789 on the Yearly Timescale, Phase II	174

4.17	Solar Analogs in NGC 6819 on the Yearly Timescale, Phase II	177
4.18	Solar Analogs in M67 on the Yearly Timescale, Phase II	181
4.19	Solar Analogs in NGC 188 on the Yearly Timescale, Phase II	181
5.1	NGC 7789 Variable Stars' Properties	187
5.2	NGC 7789 New Periodic Variable Coordinates	191
5.3	NGC 6819 Variable Stars' Properties	193
5.4	NGC 188 Variable Stars' Properties	198
5.5	Summary of Binary Sequence Activity	204
5.6	V vs B and V vs R Slopes for All Clusters	204
6.1	Summary of Nightly Activity as a Function of Age	207
6.2	Summary of Annual Activity as a Function of Age	207
6.3	Gaussian FWHMs for All Clusters	211
6.4	Ensemble Error Vs. Age	212
6.5	A_v vs A_b and A_v vs A_r Slopes for All Clusters	230
6.6	A_v vs A_b and A_v vs A_r Slopes for All Clusters	233
6.7	Results of Fit to Activity vs. Age	242

List of Figures

1.1	Age vs. Activity	14
1.2	Comparison of Blackbody Curves	16
2.1	NGC 7789	30
2.2	NGC 6819	31
2.3	M67	32
2.4	NGC 188	33
3.1	Shutter Pattern	48
3.2	MLO Flat Field	50
3.3	SITe CCD Flat Field	51
3.4	Navy CCD Flat Field	52
3.5	First Loral CCD Flat Field	53
3.6	Second Loral CCD Flat Field	54
3.7	Differential Ensemble Photometry Check	64
3.8	Differential Ensemble Photometry Re-Check	65
3.9	V vs. σ_{rms} and σ_{mean} in NGC 7789	67
3.10	V vs. σ_f/σ_{phot} and $\sigma_{rms}/\sigma_{mean}$ for NGC 7789	68
3.11	V vs. $\sigma_{rms}/\sigma_{mean}$ for NGC 7789 Randomized Data	70
3.12	Histograms of Datasets on UT 1999 Sep 13	73
3.13	Comparison of Datasets on UT 1999 Sep 13	74
3.14	Color-Magnitude Diagrams for NGC 7789.	77
3.15	Activity Index and Error for Main Sequence Stars in NGC 7789	79

3.16	Correlation Coefficient vs. V for NGC 7789	80
3.17	Mean V vs. Mean B or Mean I for Stars in NGC 7789	81
3.18	Power Spectrum for Star 2055.	83
3.19	Histogram of Periods of Maximum Power for Variables and Non-Variables in NGC 7789	84
3.20	Power Spectrum for Star 3105	85
3.21	BVI Plot of Star 3105	86
3.22	Solar Analogs in NGC 7789, Part 1.	88
3.23	Solar Analogs in NGC 7789, Part 2.	89
3.24	Mean BVI Magnitudes vs. Time for Selected Stars in NGC 7789	91
3.25	CMD for Annual V Magnitudes for NGC 7789.	92
3.26	Annual Mean V vs. B or I for NGC 7789	93
3.27	Annual V, B, and I Magnitudes Vs. Time for Selected NGC 7789 Stars	94
3.28	Differential Ensemble Photometry Re-Check	101
3.29	V vs. σ_{rms} , σ_{mean} , and σ_{phot} for All Clusters	102
3.30	V vs. σ_f/σ_{phot} and $\sigma_{rms}/\sigma_{mean}$ for All Clusters	103
3.31	Color-Magnitude Diagrams for NGC 7789.	104
3.32	Color-Magnitude Diagrams for NGC 6819	105
3.33	Color-Magnitude Diagrams for M67	106
3.34	Color-Magnitude Diagrams for NGC 188	107
3.35	Significance Index for Main Sequence Stars in All Clusters	108
3.36	Activity Index and Error for Main Sequence Stars in All Clusters	108
3.37	Correlation Coefficient vs. V for Main Sequence Stars in All Clusters	109
3.38	Correlation Coefficient vs. V for Candidate Variable Stars in All Clusters	110
3.39	Mean V vs. Mean B or Mean I for Stars in All Clusters	112
3.40	Power Spectra of All Clusters	113
3.41	Mean V Magnitudes vs. Time for Solar Analogs in NGC 6819, Part 1	115

3.42	Mean V Magnitudes vs. Time for Solar Analogs in NGC 6819, Part 2	116
3.43	Mean V Magnitudes vs. Time for Solar Analogs in NGC 6819, Part 3	117
3.44	Mean BVI Magnitudes vs. Time for Selected Stars in NGC 6819	118
3.45	Solar Analogs in M67	120
3.46	Mean BVI Magnitudes vs. Time for Selected Stars in M67	121
3.47	Solar Analogs in NGC 188, Part 1	123
3.48	Solar Analogs in NGC 188, Part 2	124
3.49	Mean BVI Magnitudes vs. Time for Selected Stars in NGC 188	125
3.50	CMD for Annual V Magnitudes for NGC 7789 and NGC 6819	126
3.51	Annual Mean V vs. B or I for NGC 7789 and NGDC 6819	127
3.52	Annual V, B, and I Magnitudes Vs. Time for Selected NGC 7789 Stars	128
3.53	Annual V, B, and I Magnitudes Vs. Time for Selected NGC 6819 Stars	129
3.54	Annual V, B, and I Magnitudes Vs. Time for Selected M67 Stars	130
3.55	Annual V, B, and I Magnitudes Vs. Time for Selected NGC 188 Stars	132
4.1	Differential Ensemble Photometry Check for All Clusters, Phase II	140
4.2	V vs. σ_f/σ_{phot} and $\sigma_{mean}/\sigma_{rms}$ for All Clusters, Phase II	141
4.3	V vs. σ_{rms} and σ_{mean} for All Clusters, Phase II	142
4.4	Color-Magnitude Diagrams for All Clusters, Phase II.	144
4.5	Significance Index for Main Sequence Stars in All Clusters, Phase II	145
4.6	Activity Index and Error for Main Sequence Stars in All Clusters, Phase II	146
4.7	Correlation Coefficient vs. V for All Clusters, Phase II	147
4.8	Correlation Coefficient for Candidate Variables vs. V for All Clusters, Phase II	148
4.9	Mean V vs. Mean B or Mean R for Main Sequence Stars in All Clusters, Phase II	149
4.10	Mean V vs. Mean B or Mean R for Active Stars in All Clusters, Phase II	151
4.11	Rotated V vs. B Plot for Active Stars in NGC 7789	152

4.12	Histograms of the Signal + Noise and the Noise in the Rotated Mean Magnitude Plots for NGC 7789, Phase II	153
4.13	Histograms of the Signal + Noise and the Noise in the Rotated Mean Magnitude Plots for NGC 6819, Phase II	155
4.14	Histograms of the Signal + Noise and the Noise in the Rotated Mean Magnitude Plots for M67, Phase II	156
4.15	Histograms of the Signal + Noise and the Noise in the Rotated Mean Magnitude Plots for NGC 188, Phase II	157
4.16	Mean BVR Magnitudes vs. Time for Selected Solar Analogs in NGC 7789, Phase II	158
4.17	Mean BVR Magnitudes vs. Time for Selected Stars in NGC 6819, Phase II	159
4.18	Mean BVR Magnitudes vs. Time for Selected Stars in M67, Phase II	160
4.19	Mean BVR Magnitudes vs. Time for Selected Stars in NGC 188, Phase II	162
4.20	Correlation Coefficient vs. V for Annual Means for All Clusters, Phase II	163
4.21	Correlation Coefficient vs. V for Annual Means of Candidate Variables for All Clusters, Phase II	164
4.22	Color-Magnitude Diagrams for All Clusters, Annual Data, Phase II.	166
4.23	Annual Mean V vs. B, R or I for Active Stars in All Clusters, Phase II	167
4.24	Interesting Stars in NGC 7789 on the Yearly Timescale, Phase II, Part1	169
4.25	Interesting Stars in NGC 6819 on the Yearly Timescale, Phase II, Part1	170
4.26	Interesting Stars in M67 on the Yearly Timescale, Phase II, Part1	172
4.27	Interesting Stars in NGC 188 on the Yearly Timescale, Phase II, Part1	173
4.28	Solar Analogs in NGC 7789 on the Yearly Timescale, Phase II, Part 1	175
4.29	Solar Analogs in NGC 7789 on the Yearly Timescale, Phase II, Part 2	176
4.30	Solar Analogs in NGC 6819 on the Yearly Timescale, Phase II, Part 1	178
4.31	Solar Analogs in NGC 6819 on the Yearly Timescale, Phase II, Part 2	179
4.32	Solar Analogs in NGC 6819 on the Yearly Timescale, Phase II, Part 3	180

4.33	Solar Analogs in M67 on the Yearly Timescale, Phase II, Part 1	182
4.34	Solar Analogs in M67 on the Yearly Timescale, Phase II, Part 2	183
4.35	Solar Analogs in NGC 188 on the Yearly Timescale, Phase II	184
5.1	NGC 7789 Periodic Variable CMD	187
5.2	NGC 7789 Periodic Variable Lightcurves	188
5.3	NGC 7789 Periodic Variable 2840	189
5.4	Large NGC 7789 Finder Chart	191
5.5	Small NGC 7789 Finder Charts	192
5.6	NGC 6819 Periodic Variable CMD	193
5.7	NGC 6819 Periodic Variable Lightcurves	194
5.8	NGC 6819 Periodic Variable 4187	195
5.9	Large NGC 6819 Finder Chart	196
5.10	Small NGC 6819 Finder Chart	197
5.11	M67 Period Variable 5833 Lightcurve	197
5.12	NGC 188 Periodic Variable CMD	198
5.13	NGC 188 Periodic Variable Lightcurves	199
5.14	Large NGC 188 Finder Chart	201
5.15	Small NGC 188 Finder Charts	202
5.16	Color-Magnitude Diagrams Showing Binary Sequences	203
5.17	Mean V vs. Mean B or Mean R for Main Sequence and Binary Sequence Stars in All Clusters	205
6.1	Significance Indices for Main Sequence Stars in All Clusters	214
6.2	Activity Indices for Main Sequence Stars in All Clusters	215
6.3	Errors in the Activity Index for Main Sequence Stars in All Clusters	217
6.4	Significance Indices for Active Stars in All Clusters	218
6.5	Activity Indices for Active Stars in All Clusters	219
6.6	Errors in the Activity Index for Active Stars in All Clusters	220

6.7	Significance Indices for Main Sequence Stars in All Clusters for the Yearly Timescale	221
6.8	Activity Indices for Main Sequence Stars in All Clusters for the Yearly Timescale	222
6.9	Errors in the Activity Index for Main Sequence Stars in All Clusters for the Yearly Timescale	223
6.10	Significance Indices for Active Stars in All Clusters for the Yearly Timescale	224
6.11	Activity Indices for Active Stars in All Clusters for the Yearly Timescale	225
6.12	Error in the Activity Indices for Active Stars in All Clusters for the Yearly Timescale	226
6.13	A_v vs A_b and A_v vs A_r for Main Sequence Stars in All Clusters	228
6.14	A_v vs A_b and A_v vs A_r for Active Stars in All Clusters	229
6.15	A_v vs A_b and A_v vs A_r for Main Sequence Stars in All Clusters	231
6.16	A_v vs A_b and A_v vs A_r for the Active Stars in All Clusters	232
6.17	Distribution of Active Stars by Spectral Type in All Clusters for Nightly Timescale	234
6.18	Distribution of Active Indices for Stars by Spectral Type in All Clusters on the Nightly Timescale	236
6.19	Distribution of Active Stars by Spectral Type in All Clusters for Annual Timescale	237
6.20	Distribution of Active Indices for Stars by Spectral Type in All Clusters on the Yearly Timescale	239
6.21	Age vs. Activity on Rotational and Yearly Timescales	240
6.22	Fit to Activity vs. Age	241
7.1	M67 with PRISM	251

List of Acronyms

ACRIM	Active Cavity Radiometer Irradiance Monitor
ADU	analog-to-digital units
BU	Boston University
CCD	charge-coupled device
DEC	declination
ERBS	Earth Radiation Budget Satellite
FWHM	full width at half-maximum
HF	Hickey-Frieden radiometer
IC	Index Catalog
IR	infrared
IRAF	Image Reduction and Analysis Facility
M	Messier Catalog
MLO	Mt. Laguna Observatory
NGC	New General Catalog
OGLE	Optical Gravitational Lensing Experiment
PRISM	Perkins Re-Imaging System
PSF	point-spread function
RA	right ascension

RMS	root-mean-square
S/N	signal-to-noise ratio
SITe	Scientific Imaging Technologies
SMM	Solar Maximum Mission
SOHO	Solar and Heliospheric Observatory
SPS	Stellar Photometry Software
USNO	United States Naval Observatory
USNOFS	United States Naval Observatory, Flagstaff Station
UT	Universal Time
UV	ultraviolet
VIRGO	Variability of Solar Irradiance and Gravity Oscillations

Chapter 1

Introduction

The Sun is variable on a wide range of timescales: from a few minutes to the years that make up a solar cycle (Lockwood, Skiff & Radick 1997; Pap et al. 1999). The Sun's irradiance, which is defined as the amount of radiant energy emitted by the Sun over all wavelengths that falls on 1 m^2 each second at a distance of 1 AU, varies from effects operating on at least three timescales: the p-mode oscillations of the Sun, individual sunspots and plages passing across the surface of the Sun and the 11-year solar cycle. All of these effects are at a very low level, less than a 1% change in the Sun's brightness. Photospheric, chromospheric, and coronal effects related to the long-term solar cycle have similar timescales (Gilliland & Baliunas 1987).

The Sun's activity and associated irradiance changes affect the Earth's climate (Lean & Rind 2001), but we do not yet know to what extent the Sun's irradiance may change over the long term. We can estimate this indirectly by studying the behavior of other stars. First, I will describe the current state of knowledge of the Sun's variability, and then what is known about the variability of other types of stars.

I have observed several open star clusters at multiple wavelengths to determine the degree of stellar activity in each star cluster as a function of spectral type. Since the open clusters range in age from 1.6 Gyr to approximately 7 Gyr, these observations will also

provide a breakdown of stellar activity by age. Consequently I will begin to understand the type of activity that might be expected from the Sun.

1.1 The Sun and Its Activity

Solar activity includes photospheric, chromospheric, and coronal activity. Photospheric activity consists primarily of sunspots, but also includes plages, faculae, granulation, and super-granulation. Sunspots are cooler (and therefore darker) regions in the photosphere caused by magnetic field activity, and are created and destroyed over periods of days to a few weeks. Chromospheric activity is dominated by plages, which are regions of bright $H\alpha$ emission generally located near active sunspots. They are longer-lasting than their associated sunspot.

More transitory activity consists of solar flares and prominences. Flares are eruptions of stellar material that occur in a few hours or less, originating from active sunspots. Prominences may be longer-lived. They consist of ionized gas that travels from the chromosphere along looping magnetic field lines and eventually falls back down to the chromosphere; they may extend far into the corona.

The majority of coronal activity is caused by variations of coronal structure. During times of low solar activity, the corona is featureless and generally isotropic. When the Sun is more active, however, the corona has gaps and streamers whose structure changes more quickly. Occasionally during periods of high solar activity, large amounts of material suddenly erupt from the corona and escape from the Sun; these are known as coronal mass ejections.

The solar cycle is a long-term cycling of solar activity, most obvious in the number of sunspots visible on the Sun at any point during the cycle. Approximately every eleven years, the number of sunspots reaches a maximum, declines to a minimum approximately 5.5 years later, and then increases again. The Sun's magnetic field switches polarity with each cycle. The Sun's total irradiance also varies on the same time scale.

Several experiments have been flown aboard spacecraft to measure the solar irradiance. The Solar Maximum Mission (SMM) found that when the cooler sunspots cross the Sun's surface, the Sun's brightness dims by as much as 0.2% (Willson et al. 1981) or approximately 2 millimagnitudes (mmag). The VIRGO experiment on the SOHO spacecraft showed that the amplitude of the variability caused by sunspots is larger at UV wavelengths than at red and IR wavelengths (Pap et al. 1999). This result is expected from the basic physics of thermal phenomena and will be expanded upon later.

The Sun's short-term variability is related to sunspots. ACRIM data show that dips in the Sun's brightness are caused by the darker sunspots that move across the Sun's surface; the younger, more complex sunspot groups have a larger effect (Frohlich & Pap 1989). VIRGO data further show that the Sun's total irradiance is affected primarily by sunspots, but that the Sun's UV irradiance is more affected by plages (Pap et al. 1999). VIRGO also confirmed that active sunspot regions cause the strongest modulation in the brightness (Pap et al. 1999).

The solar cycle is much more difficult to monitor because of its long period. According to a composite record of the Sun's irradiance (from the HF, ACRIM I and II, ERBS, and VIRGO experiments), the Sun's irradiance was 0.1% (1 mmag) higher during the sunspot maxima of 1980 and 1990 than during the minimum of 1986 (Willson & Hudson 1991).

1.2 Why is the Sun Active?

Why does the Sun have activity? What generates sunspots, plages, and the other manifestations of that activity? The accepted model of the Sun's activity is the magnetic dynamo. Differential rotation of the Sun's outer layers shears the nominally poloidal magnetic field and produces a toroidal field (Leighton 1969). During this shear, strands of the toroidal magnetic field breach the surface of the Sun and form sunspots (Leighton 1969; Parker 1955b). Eventually the fluid motions in the toroidal magnetic field regenerate the Sun's poloidal magnetic field, reversing the polarity (Parker 1955a). The cycle then begins anew.

The strength of the magnetic dynamo is determined by the depth of the Sun’s convective zone and the rotational velocity of the Sun (Noyes et al. 1984). These factors have a combined effect described by the Rossby number:

$$Ro = \frac{P_{rot}}{\tau_c}, \quad (1.1)$$

where P_{rot} is the rotation period of the Sun, and τ_c is the convective turnover time at the base of the convection zone. The convective turnover time is determined by the degree by which the Coriolis forces of rotation are introducing helicity into the motions of convection. Analytic models of the magnetic dynamo predict periodicities of solar activity that relate to the Rossby number. However, models describing the Sun’s activity fully have not yet been developed (Baliunas & Vaughan 1985). The Rossby number is a fixed quantity for the Sun; it is a way to compare the Sun with other stars, since stars with higher levels of activity will have lower Rossby numbers.

1.3 The Activity of Other Stars

1.3.1 Extending the Magnetic Dynamo Model

The magnetic dynamo model developed for the Sun should apply to any star whose structure is similar to the Sun – that is, with a convective zone. Stars with deeper convective zones will have longer turnover times (τ_c) at the bases of their convection zones and therefore will have greater stellar activity. Rapidly rotating stars will have more activity than slower spinning stars (Noyes et al. 1984).

How is stellar activity affected by the aging of a star? A star’s rotational velocity decreases over time due to magnetic braking – the magnetic fields in the star’s atmosphere and stellar wind act to slow the star’s rotation (Baliunas & Vaughan 1985; Brandenburg, Saar & Turpin 1998). Thus the Rossby number increases with age.

Skumanich (1972) used observations of the chromospheric activity in the Pleiades, Ursa Major group, the Hyades, and the Sun to show that the amplitude of variability

because of stellar activity in these stars declined as $t^{-1/2}$, where t is the age of the stars. Soderblom (1983) used lithium abundances to determine the ages of field stars; then he used observations of the rotational velocities of cluster stars as well as field stars to determine the same relationship: $v \sin(i) \propto t^{-1/2}$. However, neither of these results included observations of stars older than the Sun.

Soon, Baliunas & Zhang (1993) proposed the quantity P_{cyc}/P_{rot} , which is the period of the stellar activity cycle divided by the rotation period, as an observational equivalent to the dynamo number, which is inversely proportional to the Rossby number. When they examined the relation between P_{cyc}/P_{rot} and B-V color for the 25 years of chromospheric observations of the Mount Wilson Observatory HK Project, they found an inverse relation, and they found two populations of stars. Both populations had an inverse correlation between color and P_{cyc}/P_{rot} . However, the populations had a different relation between P_{cyc}/P_{rot} and age. One population had generally higher values of P_{cyc}/P_{rot} and were also young; the other population was older and had lower values of P_{cyc}/P_{rot} . This break between the stars seems to be the same Vaughan-Preston gap first noted by Vaughan & Preston (1980) in the chromospheric activity in stars near the Sun. They hypothesized that there was a break in dynamo efficiency between the two population of stars, at an age of 1 - 3 Gyr.

Brandenberg, Saar & Turpin (1998) also found two branches of stars that behaved similarly, using updated chromospheric data for the same stars. However, when they calculated the Rossby number from Equation 1.1 using an empirical value for τ_c and plotted it versus the chromospheric activity, they found no segregation in the stars. They proposed that P_{rot}/P_{cyc} decreases gradually as the stars age, until they reach a certain threshold, and then the stars rapidly transit to the inactive population. This transition reflects a decrease in P_{cyc} . Once the stars joins the inactive population, its activity continues to decline as $P_{rot}/P_{cyc} \propto t^{-0.35}$. The transition between populations seems to take place at ages of 2-3 Gyr (Brandenberg, Saar & Turpin 1998). The authors also found a “super

active” branch of activity upon which some very young stars fell.

Past research shows that stars of later spectral types are more active. Stars are also more active when they are younger, before their rotation slows. However, no work has been done on stars known to be older than the Sun.

1.3.2 Sun-Like Stars

The Mt. Wilson HK Project (Baliunas et al. 1995) has been monitoring chromospheric Ca II H and K line flux for approximately 100 nearby stars, some for twenty-five years. The H and K line emission increases in response to the heating produced by local magnetic inhomogeneities, such as plages. Baliunas et al. (1995) analyzed the twenty-five years’ worth of data, and found that F-type stars are nearly constant in H and K flux. Later type stars (G and K) in the survey showed both rotational and solar cycle-type activity. Some G stars exhibited very low levels of activity reminiscent of the Maunder minimum period of the Sun’s activity. A “solar cycle” period was found for forty-six of the 111 stars, with periods ranging from approximately 2.5 to 21 yrs. In addition, chromospheric flux in the H and K lines generally increased with (B-V) color.

Sun-like field stars in the solar neighborhood have also been studied to learn about their photospheric stellar activity. Lockwood, Skiff & Radick (1997) reported on ten years of observations of nearby sun-like stars in Strömgren *b* and *y*. They observed forty-one stars, approximately three-quarters of them from the Mt. Wilson HK Program. They discovered that late-F through M stars had rotational variability ranging from ~ 3 mmag to ~ 50 mmag. The yearly variability was approximately 15 mmag. They possibly uncovered “solar cycle” decade-scale variations of 30 mmag peak-to-peak, but could not find any periods. In their study, the amplitude of the yearly variability was correlated with (B-V) color.

Radick et al. (1998), combined their photometric measurements (Lockwood, Skiff & Radick 1997) with the results from the Mt. Wilson HK Project for the thirty-four stars

included in both programs. They found that the long-term activity of the nearby stars was roughly segregated by mass: those stars more massive than the Sun had low-amplitude cycles, but those stars less massive than the Sun tended to have high-amplitude cycles. They determined that both long-term and short-term (rotational) variability were correlated with the overall level of chromospheric activity of the star. Also, they observed that young, active stars tend to become fainter as their chromospheric H and K line emission increases, but older stars, including the Sun, tend to become brighter as their chromospheric emission increases. This could suggest the cause of variability for each star: younger stars decrease in brightness because starspots are the greatest influence, but for older stars, the dominant faculae cause an increase in brightness.

The “Sun in Time” project, a multi-wavelength study of nearby, solar-type stars, was begun in 1988 (see Bochanski et al. (2000)). Preliminary photometric results for rotational variability for these stars have been released; the youngest stars, ~ 70 Myr (O’Dell et al. 1995), have variations of 30 - 90 mmag, while the older stars, ~ 2 Gyr, have variations less than 10 mmag. Later results in Messina & Guinan (2002) for six G and K stars ranging in age from 130 - 750 Myr show that they have long-term cycles, similar to the solar cycle, caused by photospheric activity. The observed periods span 3 - 13 yr, with amplitudes of 60 - 310 mmag in the V band. The amplitude of variability is highly correlated with the inverse Rossby number.

The primary difficulty in observing field stars, including the Mt. Wilson HK Project stars, is determining their ages. The estimated ages of stars in the project come from indirect techniques. The abundances of certain elements such as lithium compared to abundances expected from stellar models allow an approximate age determination. Another method is to measure the rotational velocity of the star spectroscopically; younger stars have shorter rotation periods (Soderblom 1983). The amount of chromospheric emission is another indicator: younger stars are more chromospherically active. However, the reasoning in some of these methods is rather circular. A star deemed young because of

its high chromospheric activity or rotational velocity cannot then be used to show that young stars possess these properties. This is a fundamental problem not easily overcome.

Searching for stellar activity among open cluster stars is a logical next step. Compared to field stars, many properties of open clusters are well determined: age, distance, composition, and reddening. Since all of the stars in a cluster are the same age, we can observe the activity of many spectral types simultaneously. By observing clusters of different ages, we can build up a picture of how stellar activity changes for different types stars over time. Conveniently, open clusters, especially the older ones, tend to be similar to the Sun in terms of composition. However, few clusters have been observed over time periods long enough to search for this variability. Those clusters that have been observed are younger than the Sun. I present a review of those observations here.

1.3.3 IC 2391

IC 2391 is a 30 Myr old open cluster. Patten & Simon (1996) observed this cluster photometrically in V using a CCD and a photometer. They found rotation periods for 24 of 78 cluster stars from types A to M; the rotation periods ranged from $\sim 0.5 - 5.8$ d. The amplitudes of the variations were approximately 100 mmag. They also imaged the cluster with ROSAT and confirmed the correlation between fast rotation and increased coronal activity as measured by x-ray emission.

1.3.4 IC 2602

IC 2602 is a southern cluster; its age is estimated at 30 - 35 Myr (Barnes et al. 1999). Barnes et al. (1999) studied 33 stars in this cluster through a V filter for four to six weeks. Rotation periods were found for 29 of the stars from their variability due to starspots. The rotation periods ranged from 0.2 - 10.1 days, with typical photometric amplitudes of ~ 40 mmag. Little correspondence between the length of the rotation period and spectral type was found. No direct relation between amplitude and period was found, but longer

period stars tend to have small amplitudes, while shorter period stars could have large or small amplitudes.

1.3.5 α Persei

A recent investigation of the α Persei cluster by O'Dell et al. (1997) yielded rotation periods for five of nine stars in this ~ 50 Myr cluster. The stars were G- and K-type stars that were selected for their known rapid rotation. Their rotation periods were determined from one season's observations and ranged from $\sim 0.2 - 0.75$ d, with V band amplitudes of 30 - 140 mmag. Several slowly rotating stars were also observed, but the authors were unable to determine any rotation periods.

1.3.6 IC 4665

Allain et al. (1996) have studied the young (~ 70 Myr) cluster IC 4665 in the V band. They found photometric periods for eight of fifteen stars, which ranged in spectral type from F to K. The periods ranged from 0.6 - 3.7 d and the amplitudes ranged from 30 - 100 mmag.

1.3.7 The Pleiades

The Pleiades are a well-known cluster with an age of 70 - 100 Myr. The Pleiades have been studied frequently both photometrically and spectroscopically. Krishnamurthi et al. (1998), studied the Pleiades in V with five 1 m-class telescopes over three observing seasons. Variability due to rotation was detected in 21 of 36 stars observed in the cluster. The rotation periods determined ranged from 0.3 - 8.2 days with amplitudes from $\sim 50 - 100$ mmag. No pattern relating spectral type to rotation period or amplitude was seen.

Using spectroscopy of $H\alpha$ and the Ca II infrared triplet, Soderblom et al. (1993) determined $v \sin i$ for many stars in the Pleiades. The values ranged from the detection threshold of 7 km s^{-1} to $\sim 100 \text{ km s}^{-1}$. No unique correlation between rotation velocity

and spectral type was seen, but the spread in rotation velocities showed a pattern. Late-F and early-G dwarfs have a factor of five range in $v \sin i$, while late-G and K dwarfs have a factor of twenty range. A small population of stars were called ultra fast rotators, with $v \sin i \geq 30 \text{ km s}^{-1}$.

1.3.8 The Coma Star Cluster

The Coma star cluster is estimated to be ~ 430 Myr in age. Radick, Skiff & Lockwood (1990) observed the cluster in Strömgren b and y between 1984 and 1987. They detected no variability on either rotational or yearly timescales for the four F stars in their survey. They found that the four G stars in the survey were variable by ~ 7.8 mmag on rotational timescales and by ~ 15 mmag on yearly timescales.

1.3.9 The Hyades

The Hyades (approximately 600 Myr old) have been monitored for stellar activity by several research groups. Radick et al. (1987) observed 24 stars in the Hyades photometrically in Strömgren b and y and spectroscopically via the Ca II H and K lines over one season. Photometrically, they found none of the six stars earlier than F7 to be variable; they found all eighteen late-F, G and K stars to have short-term (rotational) variability with an amplitude of ~ 40 mmag and long-term variability of ~ 15 mmag. They speculate that earlier stars would also be variable with higher photometric precision.

The rotation periods that Radick et al. (1987) found ranged from approximately five days to thirteen days; the periods tended to increase with spectral type. A typical G star in the Hyades rotates three to four times faster than the Sun. Through the Ca II H and K line observations, they determined that drops in photometric brightness correspond to increases in the H and K flux, which suggests that starspots and plages coincide on the stars' surfaces.

The continuation of these observations, which resulted in twelve years of observations

of ten G and K stars, yielded similar results (Radick et al. 1995). The long-term variability was found to be ~ 7 mmag, slightly less than that found by Radick et al. (1987). Rotation periods ranging from six to eleven days were found for the stars.

Stauffer et al. (1991), observed the $H\alpha$ line on low-mass Hyades stars, since $H\alpha$ equivalent widths also indicate the amount of chromospheric activity present on a star. Comparing their data to that from the Hyades and field M dwarfs, they concluded that chromospheric activity decreases with the age of the star. They also observed that $H\alpha$ emission or absorption equivalent widths may vary with plages on the star in a manner similar to the solar cycle.

1.3.10 M67

M67 is a much older open cluster of ~ 4 Gyr. Giampapa et al. (2000) have undertaken a long-term Ca II H and K line study of over 100 solar-type stars in the cluster. Interim results, which appear to be based on observational data from a single epoch, show that the H and K emission has a much wider range than the emission seen from the Sun. Approximately 30% of the stars exhibit levels of activity that are outside of the range of activity normally seen from the Sun.

Stassun et al. (2002) searched 990 stars projected around M67 for variability in BVI. For five observing runs over two years, they found 69 variable stars. Variable F stars had an average amplitude of 16 mmag, G stars 21 mmag, and K stars 22 mmag.

1.3.11 Current Activity vs. Age Relationship

From the works previously discussed, we can summarize what is known currently about the relationship between stellar activity and age. Observations to date have focused heavily on young cluster stars or nearby field stars of not well-determined ages. Tables 1.1 and 1.2 summarize the variability of the stars previously discussed on time scales of days and years. The amplitude of variability generally declines with age, but increases with spectral

type for each age. Figure 1.1 illustrates this with the G stars.

Spectral Type	Rotational (Days)		Age	Reference
	Amp. (mmag)	Target		
G	~ 80	IC 2391	30 Myr	1
K	~ 130	IC 2391	30 Myr	1
M	~ 90	IC 2391	30 Myr	1
G	~ 35	IC 2602	35 Myr	2
K	~ 33	IC 2602	35 Myr	2
M	~ 41	IC 2602	35 Myr	2
G	~ 70	α Per	50 Myr	3
G	~ 50	IC 4665	70 Myr	4
G	~ 95	Pleiades	70 Myr	5
K	~ 96	Pleiades	70 Myr	5
M	~ 60	Pleiades	70 Myr	5
G	$\sim 30 - 90$	local dwarfs	~ 70 Myr	6
G	~ 7.8	Coma	430 Myr	7
late-F	~ 32	Hyades	700 Myr	8
G	~ 40	Hyades	700 Myr	8
K	~ 40	Hyades	700 Myr	8
F	~ 2.7	HK Project	?	9
G	~ 3.8	HK Project	?	9
K	~ 5.3	HK Project	?	9
M	~ 80	HK Project	?	9
G	< 10	local dwarfs	~ 2 Gyr	6
F	~ 16	M67	4 Gyr	10
G	~ 21	M67	4 Gyr	10
K	~ 22	M67	4 Gyr	10
G	2	Sun	4.6 Gyr	11

Table 1.1: Photometric Variability on the Rotational Timescale. It should be noted that many of the amplitudes are for single stars or averages of a handful of stars. References: 1 - Patten & Simon (1996); 2 - Barnes et al. (1999); 3 - O’Dell et al. (1997); 4 - Allain et al. (1996); 5 - Krishnamurthi et al. (1998); 6 - Bochanski et al. (2000); 7 - Radick, Skiff & Lockwood (1990); 8 - Radick et al. (1987); 9 - Lockwood, Skiff & Radick (1997); 10 - Stassun et al. (2002); 11 - Willson et al. (1981).

Spectral Type	Long-Term (Years)		Age	Reference
	Amp. (mmag)	Target		
G	~ 170	Sun in Time	130 Myr	14
K	~ 120	Sun in Time	130 Myr	14
G	~ 70	Sun in Time	300 Myr	14
G	~ 15	Coma	430 Myr	7
G	~ 60	Sun in Time	600 Myr	14
G	~ 7	Hyades	700 Myr	12
G	~ 70	Sun in Time	750 Myr	14
F	~ 2.8	HK Project	?	9
G	~ 19.3	HK Project	?	9
K	~ 11.8	HK Project	?	9
G	1	Sun	4.6 Gyr	13

Table 1.2: Photometric variability on the yearly timescale. It should be noted that many of the amplitudes are for single stars or averages of a handful of stars. References: 7 - Radick, Skiff & Lockwood (1990); 9 - Lockwood, Skiff & Radick (1997); 12 - Radick et al. (1995); 13 - Frohlich & Lean (1998); 14 - Messina & Guinan (2002).

1.4 Distinguishing Stellar Activity

One challenge is to distinguish variability caused by stellar activity from that caused by other phenomena, some of which were discussed above. Stellar activity has been monitored photometrically through a star's chromospheric activity, resulting from plages, or its photospheric activity, caused by starspots and faculae. Observations of chromospheric activity are usually made spectroscopically, targeting the Ca II H and K lines (Baliunas et al. 1995) or the $H\alpha$ line (Stauffer et al. 1991), for example.

Photospheric activity has been monitored through broad-band or intermediate-band photometric observations. This study utilized broad band photometry because the cluster stars are relatively faint, so the number of photons received must be maximized. As a comparison, the nearby solar-type stars that the Mt. Wilson Project is monitoring have $V \sim 6$. The solar-type stars in the clusters in this project have $V \sim 14$ to $V \sim 17$, which means the solar-type stars in this project are up to 25,000 times fainter. The exposure times needed to achieve adequate signal-to-noise in a moderately high resolution spectrum

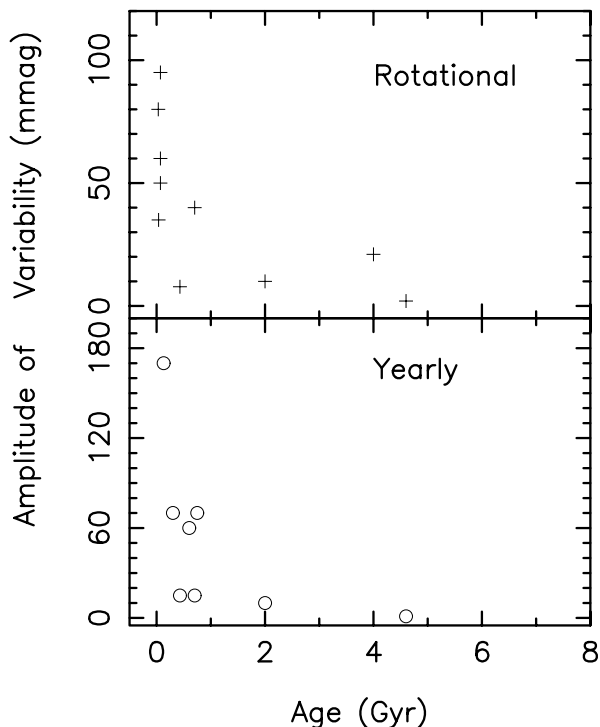


Figure 1.1: Age vs. Activity for G Stars. The crosses represent activity on the timescale of days, due to rotation. The circles represent activity on the timescale of years. A description of the data points and references are in Tables 1.1 and 1.2.

would be prohibitive. The long exposure times would also preclude monitoring many stars, since the measurements would be taken sequentially.

Two aspects of the photospheric variability should, in combination, identify its origin. First, the variability should be correlated in color. Since a starspot passing across the face of the star makes the star appear cooler and redder, all of the broad band colors we might observe should dim simultaneously. Faculae will make the star appear hotter and bluer. Figure 1.2 plots the solar spectrum for several temperatures, utilizing models by Kurucz (1992). The solar spectrum at 5870 K represents the solar faculae; 5770 K is the temperature of the photosphere; and 3900 K is the temperature of a sunspot. In addition the 75% band-passes of the Johnson/Kron-Cousins BVRI filters are plotted.

The amplitude of variability in each filter due to starspots and faculae will depend on

the relative surface area of the two phenomenon. From the figure, one can see that the spectrum of the sunspot is nearly flat over the wavelength range observed through the filters. However, the facular spectrum changes significantly over the same range. Thus, if starspots dominate the variability, the amplitude of the brightness changes should be nearly equal in all filters, but if faculae dominate, the amplitude of the brightness changes should be greatest at shorter wavelengths.

This effect is demonstrated in Table 1.3. I have adopted the approach of Fligge et al. (1998), which models the solar spectrum including the effects of sunspots and faculae by assuming the spectra of these phenomena are similar to the Sun, but at lower and higher temperatures, respectively. They then subtract flux from the spectrum according to the area of the solar disk covered by sunspots and add flux to the spectrum according to the area of the solar disk covered by faculae. I have then convolved the resulting spectrum with the BVRI filter response. By comparing the changes in flux when spots and faculae are absent to when they are present, I have determined the effects of each phenomenon on the amplitude of variability through each filter.

Surface Area	ΔB	ΔV	ΔR	ΔI	$\Delta B/\Delta V$	$\Delta R/\Delta V$	$\Delta I/\Delta V$
10% sunspot	0.1093	0.1047	0.0996	0.0923	1.04	0.95	0.88
10% faculae	-0.0124	-0.0091	-0.0076	-0.0064	1.36	0.84	0.70

Table 1.3: The amplitude of variability in each filter, assuming the star has the indicated fraction of its surface area covered by either spots or faculae. As in Figure 1.2, the photosphere is assumed to have a temperature of 5770 K, the faculae 5870 K, and the sunspots 3900 K.

This calculation obviously makes a number of assumptions. I have assumed that other stars will have starspots and faculae of the same temperatures as on the Sun. The spectra of the spots and faculae may not be identical to the solar spectrum; indeed, the stellar spectra of the unblemished photosphere will not be identical to the Sun's. The stars observed will also not manifest only starspots or faculae, but will have some combination of the two phenomena. However, Table 1.3 can be used as a guide: if the amplitude of the

variability is higher at lower wavelengths, then faculae are the primary contributor, but if the amplitude is roughly constant at all wavelengths, then spots are the main contributor.

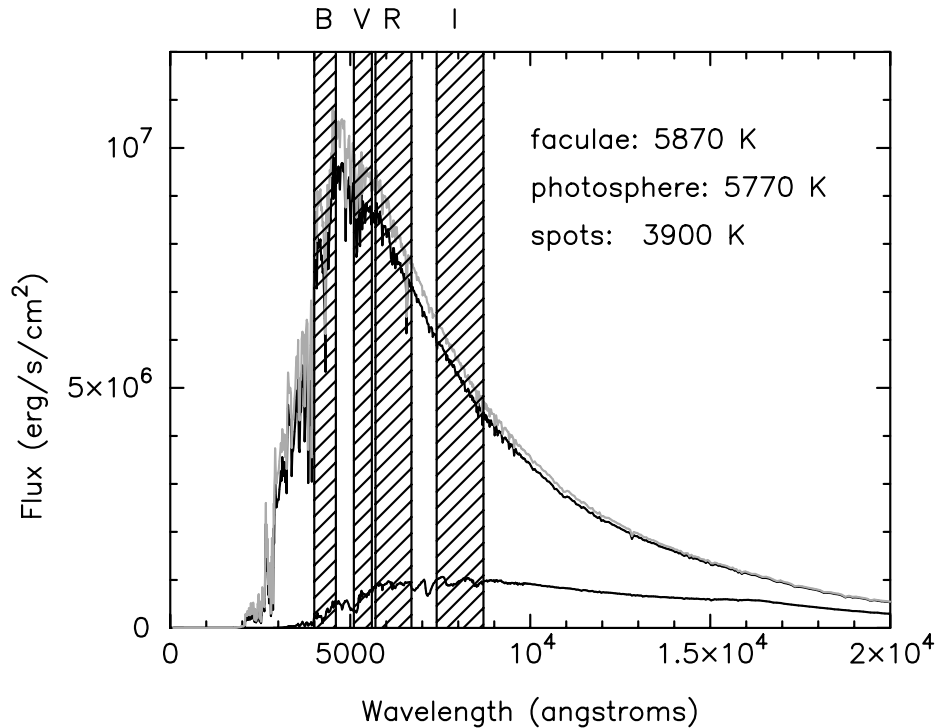


Figure 1.2: Blackbody curves at three temperatures representing faculae (in gray), the photosphere, and sunspots, in order of decreasing temperature. The 75% band-passes of the Johnson/Kron-Cousins BVRI filters are also plotted. Solar spectra models are by Kurucz (1992).

The inclination of each star will affect its amplitude of variability. Models by Unruh et al. (2000) show that the amplitude of variability over a solar cycle may increase by a factor of three or more if a star is observed nearly pole-on. In such a case, the contrast of facular regions is enhanced since they appear on the stellar limb; the contrast of starspots is diminished, but the faculae are the dominant effect. The inclinations of the individual stars in the program clusters have not been determined, so this effect must be kept in mind.

Another aspect of the variability is its timescale. The timescale of any variations will depend on the the rotation period of the stars, the evolution of the active regions on the stars, and any long-term cyclic behavior. While I might begin to see signs of long-term behavior, timescales of many years will not be a dominant effect in the present study since I only have eight years of data. The assumed timescale of active region evolution on old solar-type stars is based on solar observations, which show that active regions on the Sun last from hours to a few months, with most surviving for only one solar rotation. Many studies of RS CVn binaries (such as Mohin et al. (1985); Hall, Henry & Sowell (1990); Hall et al. (1991); Rodonó & Cutispoto (1992); Strassmeier (1994); Lanza et al. (1998)) indicate that their active regions evolve over periods of months and even years; however, these stars may be “over active” due to the synchronization of their rotation with their orbital periods, which are on the order of days. Analysis of the light curves of BY Dra binaries (for example, Oskanyan et al. (1977); Rodonó & Cutispoto (1992)) show that these stars also have active regions which evolve over weeks to months. Both types of binaries are usually followed photometrically, which means that their starspots are being observed. The Mt. Wilson HK Project stars have active region lifetimes of about a month to several years (Donahue, Dobson & Baliunas 1997); these stars are similar to the Sun and also to the stars of primary interest in NGC 7789. Finally, Lawrence (1987) shows that the lifetimes of large plage complexes is 1-3 solar rotations (about 30 - 80 days) and the lifetimes of large sunspot complexes is shorter, less than two rotations (50 days).

Following the work of Soderblom (1983), one would expect the stars in the youngest cluster, NGC 7789, to rotate in about twelve days and the stars in the oldest cluster, NGC 188, to rotate in about 32 days. However, the variability will not result in a simple light curve with a well-defined period; the effect of starspots being created and destroyed and their random drift across the stellar disk will make the light curve quasi-periodic at best.

1.5 Technical Challenge

The technical challenge is to measure the extremely small fluctuations we expect to see from the cluster stars. In this section, I will review work done by other researchers on the problem of ultra-high precision photometry.

1.5.1 General CCD Data Reduction Procedure

Others are also currently pushing the limits of photometric precision. Each group has researched the basic noise sources in photometric measurements and developed similar reduction procedures. The three groups are: Hans Kjeldsen and Soren Frandsen of the Aarhus University in Denmark; Mark Everett and Steve Howell of the Planetary Science Institute; and Ronald Gilliland and Timothy Brown, of the Space Telescope Science Institute and the High Altitude Observatory, respectively. I will begin by describing the reduction process outlined by Gilliland & Brown (1988, hereafter GB88), and then discuss how the other groups' procedures differ.

GB88 sets out a detailed reduction prescription. In this, the first of their high-precision papers, they observed M67 with a 0.9 m telescope and a CCD. They observed only one field in the cluster and used exposures of one minute in duration.

The first step of data reduction according to GB88 is to make some standard corrections to an image. They caution that not all of these standard corrections are necessary for every CCD and that applying unnecessary corrections can in fact add noise to the resulting photometry. They use the overscan section of the CCD to make a base level correction and then use the average of numerous bias exposures to determine the bias pattern, which they subtract from their image. After averaging several long dark exposures, they scale the average dark to one minute exposure time and also subtract it from the image. Then they correct for any nonlinearity in the CCD. Finally, they divide the images by a flat field which is the average of many flat fields. The standard corrections applied in this project and performed with IRAF include overscan subtraction, bias pattern subtraction, and a

flat field correction, usually using sky flat fields.

Following the procedure of GB88, the next major step is the measurement of the magnitude of each star. GB88 remove the sky contribution to each pixel by interpolating sky values measured in a grid over the CCD. Then they proceed to measure magnitudes using weighted PSF fitting in an iterative manner:

1. They fit a generalized Lorentzian function to approximately a dozen bright stars to determine an analytic PSF.
2. The Lorentzian determined in the previous step is fixed in shape and fit to the same stars; the residuals from the fit are saved.
3. The residuals are convolved with a grid of pixels.
4. The sum of the analytic PSF and the residuals is fit to approximately 25 clean stars in order to find their magnitudes and positions.
5. A model of the star positions is generated.
6. All stars are re-fit using the analytic PSF plus the residuals.
7. The variance of the photons received by each pixels is found as a sum of terms due to noise in the calibrations.
8. Ensemble photometry is performed: the median magnitude of approximately eleven stars are used as a standard, and each star's magnitude is differenced from it. The stars chosen for the ensemble are similar in color to the target star and are located near the target star in the CCD image.

Kjeldsen & Frandsen (1992, hereafter KF92) follow the same basic calibrations, excluding the determination of the sky background. They find the sky background in an iterative process while performing PSF fitting photometry. First they find the local sky background around each star. Then they do PSF fitting photometry and remove the star

from the image. Repeating this process with all stars, the image is eventually blank and consists only of the sky background. They redetermine the sky background from the blank image. Then, knowing the true sky background, the stars are returned to the image and aperture photometry is performed. Any difference between the aperture and PSF fitting photometry is used to correct the PSF magnitudes.

Everett & Howell (2001, hereafter EH01) follow a procedure similar to GB88, with the important exception that they do not perform PSF-fitting photometry. Since they are not working with crowded fields, they perform aperture photometry exclusively and discard crowded stars. Once they have magnitudes measured from aperture photometry, they perform ensemble photometry in a similar manner to GB88, adding an iteration of this step to ensure that none of the ensemble stars are variable. They do not choose the ensemble stars based on the target star’s color.

All three groups have demonstrated that their reduction procedures yield similar precisions. Using a 0.9 m telescope, GB88 achieved precisions of 1.5 mmag for $V=12-13$ stars with integrations of one minute. Using the Nordic Optical Telescope, KF92 got precisions of 1 mmag with one minute of integration time. With a 0.9 m telescope, EH01 achieved precisions of 2 mmag for $V=14$ stars with three minutes of integration time.

1.5.2 Strategies for Maximizing S/N

All of these studies have resulted in a number of “lessons learned” about how to perform high-precision photometry. The first requirement is to collect as many photons as possible in order to reduce the noise from Poisson statistics (Newberry 1991), which is why some have suggested or already performed observations on defocused stars (Kjeldsen & Frandsen 1992; Howell & Everett 1999); defocusing the telescope spreads the stellar images over more pixels, which allows for longer integration times. Other ways to increase the number of photons received is to use broader filters, to increase exposure times, and to use a CCD with a high quantum efficiency (Newberry 1991).

Proper flat-fielding is critical for high-precision photometry. In order not to degrade the S/N, flat fields should have a much higher electrons/pixel total than any of the objects of interest (Newberry 1991). The flat fields should also be illuminated with the same spectrum as that of the program object (Howell & Everett 1999) to elicit the same spectral response from the CCD. Note, however, that if the telescope could be guided perfectly such that the light from the object of interest always falls on the same pixels, flat fielding would not be important as long as ensemble photometry was used (Gilliland & Brown 1988); in such a case, the differences in sensitivity of the pixels would simply make individual ensemble stars seem brighter or fainter by a constant amount.

Minimizing the amount of noise due to the sky background is another important consideration. This could be done by observing only during dark time (Newberry 1991), using a CCD with a low dark current (Newberry 1991), minimizing scattered light in the telescope setup (Newberry 1991; Kjeldsen & Frandsen 1992), and using filters that exclude night sky lines (Newberry 1991). Also, if aperture photometry is to be performed, the apertures should be chosen according to each star's brightness in order to ensure that the per pixel noise is dominated by Poisson statistics. If a star is bright, a large aperture is needed to lower the Poisson noise; if the star is faint, a small aperture is needed to lower the sky noise (Everett & Howell 2001).

The choice of CCD is also important. A CCD with low readout noise and gain will increase the signal-to-noise ratio (Newberry 1991). Also choosing a CCD that is well-matched to the telescope to provide a pixel scale that will adequately sample the stars' PSFs can be crucial, especially if PSF fitting photometry is to be done (Howell & Everett 1999). This also is important due to the variations in sensitivity with color that each pixel has (Howell & Everett 1999).

More subtle sources of noise that may be important include: gain variations (Gilliland & Brown 1988; Howell & Everett 1999, both within pixels and across the CCD), bad star centers during the photometry (Kjeldsen & Frandsen 1992), changes in the PSF

across the CCD (Kjeldsen & Frandsen 1992; Gilliland & Brown 1992), CCD shutter variations (Kjeldsen & Frandsen 1992), integration time variations (Kjeldsen & Frandsen 1992), and fringing (Kjeldsen & Frandsen 1992).

Atmospheric scintillation and transparency act to reduce the precision of photometry. Scintillation is a small change in the object’s brightness due to changes in the refractive index of the atmosphere that focus the light. Following the Young (1967) scaling law for low-frequency scintillation,

$$\sigma = 0.09D^{-\frac{2}{3}}X^{\frac{7}{4}}(2t)^{-\frac{1}{2}}\exp\left(-\frac{h}{h_o}\right), \quad (1.2)$$

where σ is the RMS error in the intensity in magnitudes, D is the aperture diameter (in cm), X is the air mass, h is the observer’s height above sea level (in m), $h_o \approx 8000$ m is the atmospheric scale height, and T is the integration time in seconds. For the Perkins telescope, $D = 182.88$ cm and $h = 2206$ m. Table 1.4 gives a sampling of σ in millimagnitudes for typical airmasses (X) and integration times (t). This scaling law applies for timescales longer than a few seconds (Dravins et al. 1998). The aperture size of the Perkins telescope filters out the highest frequency scintillation effects; most of the power of the scintillation noise is in the 1 - 10 Hz range (Dravins et al. 1998).

T(s)	X					
	1.0	1.2	1.4	1.6	1.8	2.0
10	0.474	0.652	0.854	1.079	1.326	1.594
30	0.274	0.394	0.493	0.623	0.766	0.921
60	0.194	0.266	0.349	0.440	0.541	0.651
90	0.158	0.217	0.285	0.360	0.442	0.531
120	0.137	0.188	0.247	0.311	0.383	0.460

Table 1.4: The RMS error in intensity for the Perkins telescope due to scintillation is given in millimag for a range of airmasses and integration times.

Since the refractive index of air is a function of wavelength, the amplitude and time of arrival of scintillation noise also changes with wavelength. However, the dependence of scintillation on wavelength becomes negligible for apertures larger than 20 cm (Dravins et al. 1997b).

Observations of binary stars by Dravins et al. (1997a) have shown that although the brightness changes of the binaries due to scintillation is $\sim 15\%$ smaller than that of single stars, differences between the components (separated by 2 - 8") are noticeable. Consequently, differential ensemble photometry, even with an ensemble of stars close to the target star, may not compensate for scintillation effects.

Changes in atmospheric transparency will cause changes in the extinction of the stars observed. The assumption commonly made is that any changes in transparency will be gradual in both time and across the field of view. Differential ensemble photometry should correct for this effect (for example, GB88).

1.5.3 Specialized Procedures

Some groups have developed some specialized procedures for the specific needs of their various projects. Honeycutt (1992) developed what he called "inhomogeneous ensemble photometry," which is similar to the ensemble photometry discussed previously, except that the ensemble is not composed of the same stars from frame to frame. This procedure was developed for an automated observing program where an astronomer could not check that exactly the same field was observed each night.

Howell & Jacoby (1986) experimented with a method of time-resolved photometry whereby the star(s) of interest trailed across the CCD. The advantage of this method is that the time resolution can be quite good, ~ 15 s. The disadvantages are that the sky background builds up throughout the exposure, star trails can start to overlap each other if too many stars are in the field, and added processing difficulties.

Alard & Lupton (1998) have developed a method they call "optimal image subtraction" to search for changes in brightness in the stars in two (or more) images. They choose a reference image that is well-exposed and with good seeing. Then they degrade this reference image to the seeing of each image they are searching and find the difference between the two images. Any residual brightness in a star tells how much the star's brightness

changed in the time interval between the two images. This method was developed for use in the crowded fields of microlensing surveys and was demonstrated by analyzing images from the OGLE II project. They found several periodic variables and achieved a precision of 10 mmag. A more flexible version of this method (Alard 2000) allows the core of the reference star images to vary spatially.

1.5.4 Examples of High-Precision Photometry

Typical applications of high-precision photometry include: variability in stars due to stellar activity, transits by extra-solar planets, asteroseismology, or other types of low-amplitude variable stars, such as δ Scutis and rapidly-oscillating peculiar A (roAp) stars. I will give some examples of high-precision work in each subject, including discussion of the precision reached in lab settings.

Stellar Activity

Radick, Skiff & Lockwood (1990) observed the Coma Cluster with a 0.5 m telescope and photomultiplier and got night-to-night precisions of 4 mmag. Radick et al. (1987) observed the Hyades with the same setup and achieved a night-to-night precision of 3 mmag. Lockwood, Skiff & Radick (1997) observed solar-analog field stars with the same setup and got precisions of 1.6 mmag for individual exposures. Ongoing observations of M67 by Roberts, Craine & Giampapa (2000) using a 0.5 m telescope and a CCD are achieving precisions of 4 mmag per 180 s exposure.

Transits by Extra-Solar Planets

Henry (1999) has used a program with automated telescopes and photomultipliers to search for transits. He has achieved precision as good as 1 mmag for single measurements and seasonal mean precisions of ~ 0.15 mmag. The OGLE-III program has observed 42 transits of stars observed toward the galactic center (Udalski et al. 2002); the masses

of the transiting bodies suggests that the objects range from red stars to brown dwarfs to large gas giant planets. They observed in the I band using a CCD and followed the data methods of Alard & Lupton (1998) and Alard (2000). They achieved precision of ~ 2.5 mmag for individual measurements of their brightest (13th mag) stars.

Asteroseismology

Kurtz & Balona (1984) observed α Circinus with three 0.5 m class telescopes in two colors with photomultipliers to look for signs of pulsations. They achieved precisions of 2 mmag in the best cases, for individual exposures of 20 s. Belmonte, Perez Hernandez & Roca Cortes (1990) observed an F star with 1.5 m telescopes and photomultipliers to get a 184-hr time series. The precision they achieved over the length of the time series was 2.6 mmag.

A major effort to detect pulsation modes in stars in M67 was chronicled by Gilliland et al. (1991), Gilliland & Brown (1992), and Gilliland et al. (1993). In 1987, using a 0.9 m telescope, Gilliland & Brown (1988) got noise levels of better than 1 mmag for 11th magnitude stars with one minute integrations, but did not see signs of pulsations. Gilliland et al. (1991) describes observations of M67 with five 1 m-class telescopes over a period of two weeks. They reached a precisions of 0.1 mmag over the time series for the best stars, but did not find pulsations. The next attempt, with several nights on a 2.1 m telescope, is detailed in Gilliland & Brown (1992); precisions of $0.4 \text{ mmag min}^{-1}$ were reached. The most massive effort is described in Gilliland et al. (1993), where twelve stars in M67 were observed with seven 4 m-class telescopes over seven nights. In the best cases, precisions of $0.25 \text{ mmag min}^{-1}$ were reached, and the time series showed some signs of pulsations, but nothing unambiguous.

Variable and Pulsating Stars

δ Scuti stars have always needed high-precision photometry in order to separate their various pulsation modes. Mantegazza & Poretti (1990) observed an 8.7 mag δ Scuti with a 0.5 m telescope and photomultiplier and got a precision of 5.3 mmag per exposure. Breger, Balon & Grothues (1991) observed another δ Scuti with a similar setup and achieved precisions of 2 mmag per exposure. Poretti (1991) observed a 7th magnitude δ Scuti with a similar setup and got a precision of 3.3 mmag per exposure.

Kurtz et al. (1989) observed a roAp star using a photomultiplier. They got precisions of 1 mmag in the best cases with exposures of 40 s.

Lab Measurements

Lab setups have the advantage of tightly-controlled conditions. Noise sources may be more easily determined and eliminated. Buffington, Hudson & Booth (1990) got precisions of 0.1 mmag per exposure in the lab. They noted photometric noise correlated with the slightly oscillating temperature of the dewar and slight movements of their “star” image on the CCD.

Several lab simulations were performed during the development of the Kepler satellite project. Jenkins et al. (1997) performed lab tests, using a CCD that received a flux of 1.9×10^9 photons s^{-1} and summing 20 2.5 s images. With the resulting 9.6×10^{10} photons, they achieved precisions of 0.003 mmag. More realistic simulations, including stars of different brightnesses and noise sources, are detailed in Koch et al. (2000). Using five hour integrations including all noise sources, their reduction got precision as good as 0.005 mmag for 9th to 14th magnitude stars. They also note of their six to fourteen day tests: “Small long-term changes in the temperatures of the CCD and its internal mount, and the wall and base of the CCD dewar, were found to significantly affect the spatial stability of the images.”

Borucki et al. (2000) describe tests of a photometric system consisting only of a camera

lens and CCD for use in finding transits by extra-solar planets. They achieved precisions of 2 mmag in an hour of integration on 9th to 13th magnitude stars.

1.6 Goals

The Sun's irradiance varies on timescales of days to years because of photospheric manifestations of solar activity, specifically sunspots and faculae. Since the data on the Sun's past behavior is limited, it is not clear whether the current amplitudes and timescales of variability are typical. Observations of the behavior of other stars similar to the Sun in mass, composition, and age can build a picture of the range of activity possible on the Sun. The activity of nearby field stars has been observed for decades in the Mt. Wilson HK Project, but these stars do not have well-determined ages. Open clusters have very good age estimates, but the stars in them are too faint to effectively observe spectroscopically. The stars in clusters that have been observed using broad-band photometry are all younger than the Sun.

The goal of the project is to address the following issues:

- How does the character of photospheric activity depend on age?
- How does the character of photospheric activity change with spectral type?
- How is the photospheric activity influenced by binary companions?
- Can rotation periods be determined for any stars, based on their activity?
- Can any long term trends be seen in the data similar to the solar cycle?

Because of the age of these clusters, any binary stars will have circularized and synchronized their orbits (Keppens 1997), but they may have different rotation/orbital periods than the nominal single star in the same cluster.

The data accumulated in this program also may yield some “bonus” results. For the smaller selection of stars that have been observed since 1996, long-term trends in brightness

similar to the solar cycle may be uncovered. A few transits by extra-solar planets may be observed. However, the photometry will not be precise enough to be able to detect acoustic oscillations of the type that are studied in asteroseismology.